Quantitative thermoacoustic image reconstruction of conductivity profiles

Olumide Ogunlade*, Ben Cox, Paul Beard
Department of Medical Physics & Bioengineering, Gower Street, University College London, WC1E 6BT UK

ABSTRACT

A numerical inversion scheme for recovering a map of the absolute conductivity from the absorbed power density map that is conventionally reconstructed in thermacoustic imaging is described. This offers the prospect of obtaining an image that is more closely related to the underlying tissue structure and physiology. The inversion scheme employs a full 3D full wave model of electromagnetic propagation in tissue which is iteratively fitted to the measured absorbed power density map using a simple recursive method. The reconstruction is demonstrated numerically using three examples of absorbers of varying geometries, tissue realistic complex permittivity values and noise. In these examples, the reconstruction is shown to rapidly converge to within good estimates of the true conductivity in less than 20 iterations.

Keywords: Quantitative, Thermoacoustic, Photoacoustic, Image reconstruction, Permittivity, Conductivity

1. INTRODUCTION

Thermoacoustic imaging is a hybrid imaging modality based on the absorption of short pulses of radio frequency or microwave radiation by tissue. This absorption causes a rapid localised increase in pressure which in turn gives rise to propagating ultrasound waves. By recording these waves at multiple spatial points over the tissue surface an image of the tissue can be reconstructed.

The interaction between tissue and the incident electromagnetic field is based on the dielectric properties of the tissue: specifically, its complex permittivity ($\varepsilon^* = \varepsilon' - j\,\varepsilon''$). The real part represents an energy storage term while the imaginary part represents the total dissipative effects in the tissue and is proportional to the conductivity. A conventional thermoacoustic image can, with some assumptions, be taken to represent a map of the power absorbed per unit volume which is the product of the tissue conductivity and the square of the magnitude of the electric field. The goal of quantitative thermoacoustic imaging is to recover a map of the conductivity from the absorbed power density. This is advantageous for two reasons. Firstly, the conductivity is an intrinsic property of the tissue as it is related to ionic concentration and thus a closer representation of the tissue constituents than the absorbed power density. Secondly, by recovering a map of conductivity, the deleterious effects of the spatial variation of the electric field distribution are avoided. This spatial variation is due to several factors. The first is the well-known exponential decay due to attenuation as the electromagnetic wave propagates through a lossy medium. The second is the reflection which occurs at the interface of tissues with different values of real permittivity, for example at the skin-muscle interface. Another factor is the beam spread from the antenna. At microwave frequencies, the size of the antenna is of the order of half a wavelength or greater thus dictating the minimum lateral dimensions of the illumination, with the beam diverging with distance from the antenna. The final contribution to the spatial variation of the electric field is due to the fact that thermoacoustic imaging is almost always performed in the antenna near field where the field distribution varies rapidly with distance, especially in the reactive near field. The near field of an antenna which has largest dimension D extends to a distance of approximately $2D^2/\lambda$ away from an antenna, where λ is the wavelength of the microwave excitation. For example, at 3GHz a typical waveguide antenna used for thermoacoustic imaging has dimensions of 72 by 34mm[1] such that its near field extends to a distance of 10cm from the antenna.

*ogunlade@medphys.ucl.ac.uk

Photons Plus Ultrasound: Imaging and Sensing 2012, edited by Alexander A. Oraevsky, Lihong V. Wang,
Proc. of SPIE Vol. 8223, 82230R · © 2012 SPIE · CCC code: 1605-7422/12/$18 · doi: 10.1117/12.908858

The aim of this work is to recover a map of the conductivity of the tissue by fitting a full wave 3D Electromagnetic model of the electric field distribution to the measured absorbed power density using a fixed point iterative scheme. Section 2 discusses the dielectric properties of tissues. Section 3.1 describes the forward model used in the inversion scheme in order to generate an electric field distribution for a given conductivity distribution. In section 3.2 the method of generating simulated measured absorbed power density data is presented and section 3.3 describes the inversion scheme used to recover the conductivity from the simulated measured data. Section 4 presents results of a number of numerical examples.

2. MICROWAVE-TISSUE INTERACTIONS

The power absorbed per unit volume P_d in the presence of an applied electric field E is given by

$$P_d = \sigma \,|\, E(\sigma, \varepsilon^{'} \,|^2 \qquad (1)$$

where σ is the conductivity and is related to the imaginary part of the complex permittivity of the tissue by the expression $\varepsilon'' = \sigma/(\omega\varepsilon_o)$ where ω is the angular frequency and ε_o is the relative permittivity of free space. In thermoacoustic imaging, the reconstructed image is taken to represent P_d assuming an exact reconstruction and a known Grueneisen coefficient distribution.

The dielectric properties of tissue at microwave frequencies are dominated by the relaxation of water molecules which have a high value of ε′. As a result, tissues can be broadly grouped based on their water content, with adipose dominated tissue having the lowest ε′ values. The conductivity of tissue in eqn. 1 is made up of a contribution due to ionic conductivity which involves the motion of ions, as well as a contribution from loss due to dipolar rotation which is represented by an equivalent conductivity. The values of ε′ and σ in tissue are therefore frequency as well as temperature dependent[2]. The values of ε′ and σ for a number of tissues, at 3GHz and room temperature, are tabulated in Table 1[3]

Table 1. Dielectric properties of biological tissues at 3GHz.

Tissue	**ε′**	**σ (S/m)**
Physiological fluid	67.8	2.96
Blood	57.0	3.04
Muscle	52.0	2.14
Small Intestine	53.3	3.63
Tongue	51.8	2.23
Inflated lung	20.0	0.97
Breast fat	5.0	0.17
Air	1.0	0.00

The local electric field distribution within tissue is dependent on both ε′ and σ of surrounding tissue regions. If the ε′ is known and spatially invariant, then the electric field distribution and consequently the absorbed power density is a function of the conductivity only. Such an assumption of constant ε′ is reasonable for a range of high water content tissue as tabulated in Table 1. For example when imaging blood vessels a value of ε′ = 55 for both blood and the smooth vascular muscle is reasonable.

3. METHOD AND IMPLEMENTATION

3.1 Forward model

The forward model is based on a commercial, industry standard electromagnetic solver - CST®. The software solves the full vector form of Maxwell's equations for any arbitrary 3D geometry using the finite element method. This is in contrast to the 2D scalar approximations to the Helmholtz equation previously reported[7, 8]. Such scalar approximations are only valid in the far field of the antenna where the E field is essentially planar. Figure 1 shows a schematic of the geometry that was modeled. The antenna radiates into a homogeneous medium usually oil or some matching liquid. The absorber are enclosed within a cuboid which is immersed into the oil or matching liquid. In the example shown in figure 1, two absorbers, one a solid cylinder and the other a rectangular shaped volume, are located within a cuboid which is positioned 20 mm away from the aperture of a rectangular waveguide antenna of dimensions of 72 mm by 34 mm. The solver uses an adaptive meshing system such that the mesh (Fig. 1C) is refined until convergence (of the scattering parameters or of the propagation constant) is reached. Areas with large surface current, small features and high values of ε′ will have a greater mesh density. The maximum element size can be defined, thus allowing the user to effectively vary the total number of elements in the mesh.

Perfectly matched layer (PML) boundaries exist on the outside of the bounding region, such that a wave incident on it encounters minimal reflection, thus simulating an open boundary. If the structure is symmetric, a plane of symmetry can be used to reduce the computation time. The entire solver is controlled externally from a MATLAB code using a VBA based script.

3.2 Simulated measured data

To generate a simulated measured absorbed power density map, the forward model is run for a specific distribution of absorbers with typical values of conductivity found in high water content tissues. To mitigate against the 'inverse crime' of using the same model used in the inversion to generate the simulated measured data, a smaller number of mesh elements (approx. 50,000) were used when generating the absorbed power density map P_d compared to the approximately 150,000 elements used when running the forward model in the inversion scheme. This reduction in the number of elements reduces the accuracy of the absorbed power density map and is akin to adding non Gaussian noise to it. The resulting SNR ranged from 11dB to 42dB. In addition to the noise due to the reduction in the number of mesh elements, Gaussian noise was added to the absorbed power density map where stated in the examples described in sections 4.1-4.3.

3.3 Inversion scheme

Figure 2 shows a flow chart of the inversion scheme used. This is based on the fixed point iterative method described in reference 4. The domain over which we wish to recover quantitative information is the volume of the cuboid which contains the absorbers as depicted in figure 1. First, the value of ε′ throughout this domain is assumed constant and is fixed at 55 – this assumption is made in order to ensure a unique solution as the electric field amplitude is a function of both ε′ and σ. The size of this domain was 6 mm by 6mm by 34mm with each voxel being 0.2 mm by 0.2mm by 34mm The iteration then begins by setting the σ of all the voxels to zero and running the forward model to obtain the distribution of the electric field. A first estimate of the σ of each voxel is then obtained by rearranging eqn. 1 as follows

$$\sigma = \frac{P_d}{|E|^2 + \eta} \tag{2}$$

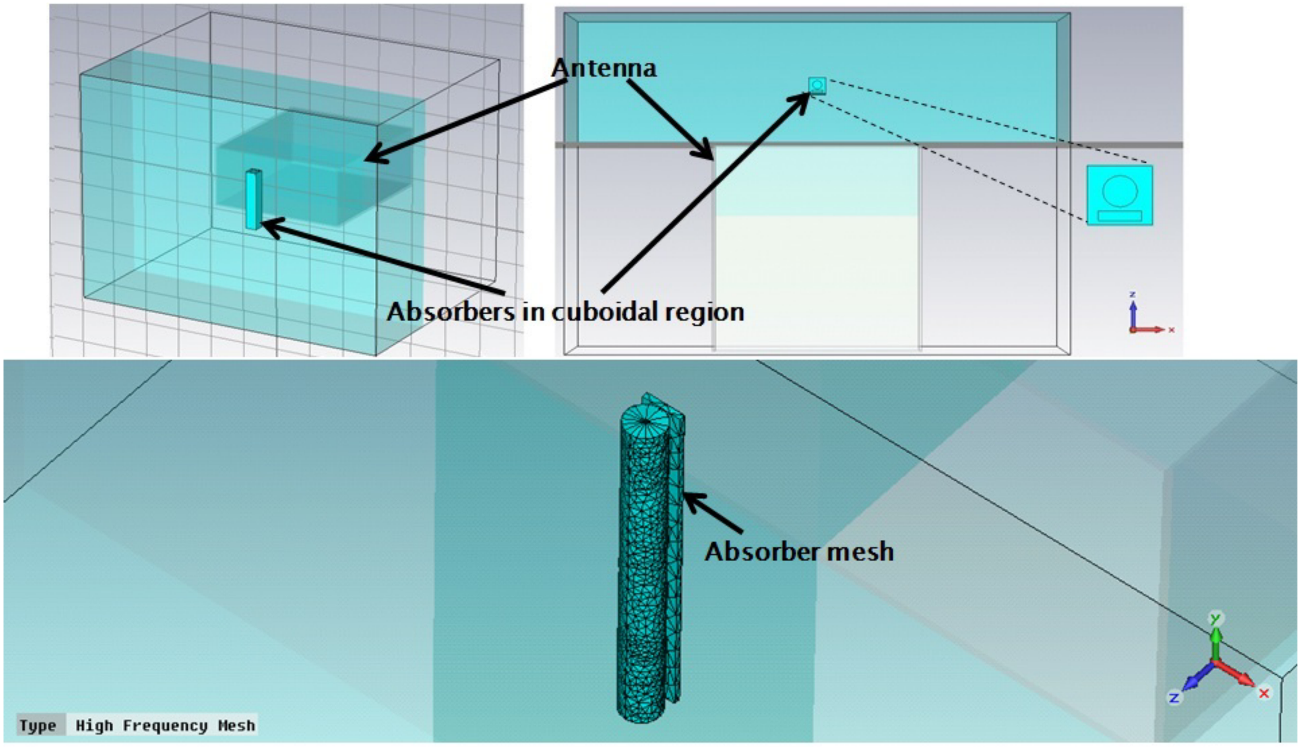

Figure 1. Schematic showing the geometry and location of the antenna, the sample mesh and the cuboidal region in which the absorbers are located – for illustrative purposes a solid cylinder and a rectangular shaped absorber are shown.

where η is a regularisation parameter and is required to prevent the result from 'blowing up' in the areas where the SNR is small, albeit at the expense of slower convergence. The value of the conductivity in each voxel is then updated with the new estimate and the forward model is re-run. This process is continued until the difference in conductivity between successive iterations (i) is less than a tolerance value. The average time taken for a single iteration was one hour on a Pentium 4 PC having 2.5GB of RAM.

4. RESULTS AND DISCUSSION

4.1 Example 1

The first example was chosen to illustrate the ability of the inversion scheme to recover the shape of circular and rectangular absorbers. Figure 3A shows the true conductivity distribution. Figure 3B shows the simulated measured absorbed power density map (P_d) produced by the conductivity distribution in figure 3A. This absorbed power density map (P_d) is before being downsampled onto the coarse voxel size used in the inversion. Note that the direction of the incident E field is along the +z axis such that the antenna is located at the bottom of the image. Due to the significant spatial variation of the incident field, the contrast distribution in P_d differs significantly from that in Fig. 3A with the boundary of the rectangle barely visible and significant contrast variation within the circular absorber. Note also that the absorbed power density in figure 3B appears to increase with increasing distance from the antenna. This somewhat counter-intuitive observation is due to the reflection arising from the discontinuity between the ε′ of the reconstruction domain (55) and that of the oil (2.45) into which the domain is immersed. Added noise is present in P_d due to the reduction in the number of elements of the mesh. The map of $|E|^2$ produced at the final iteration is shown in Fig. 3D. The recovered conductivity map after 13 iterations is shown in Fig. 3C. This illustrates reasonable agreement with the true conductivity distribution in figure 3A. However there is in fact a small discrepancy between the two as illustrated in figure 3E which shows a vertical profile at x=0 through the recovered and true conductivity maps. It is clear that the accuracy of the recovered conductivity reduces at locations where the |E| field distribution is low. The convergence of the iterations is shown in Fig 3F, where the error is defined as the difference in recovered conductivity for successive iterations summed over all the voxels. The pixelation at the edges of the recovered conductivity map presented in Fig. 3C of the circle is because the simulated measured data though generated with finer voxels, is downsampled to the coarse voxel size used in the inversion

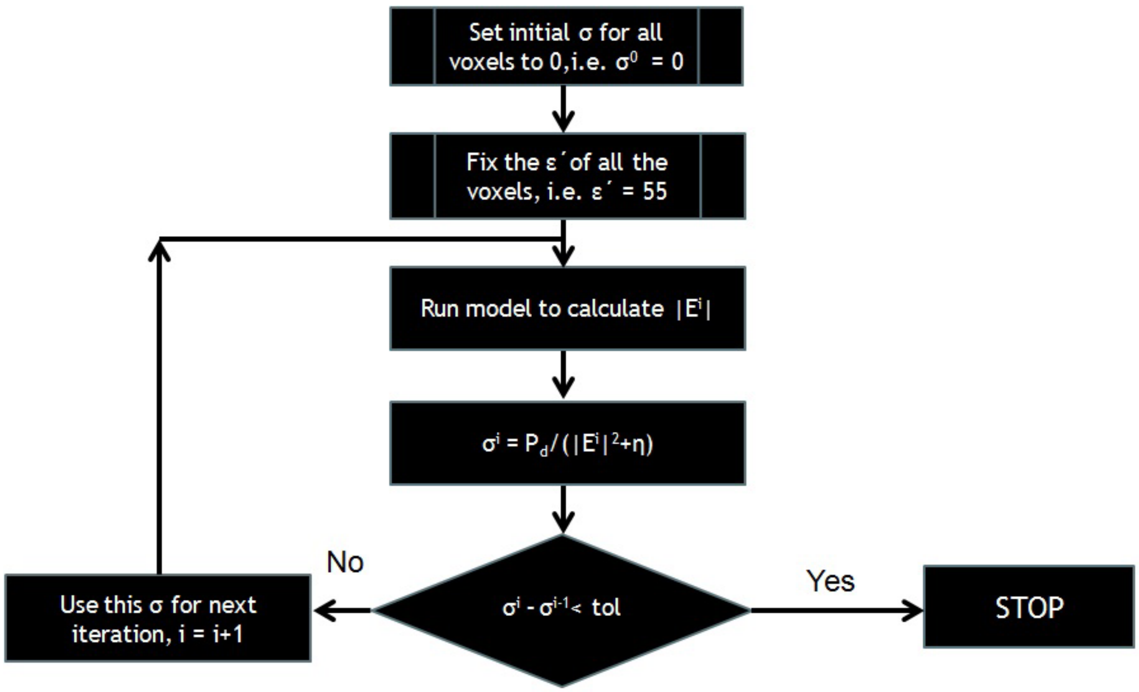

Figure 1. Flow chart showing the algorithm of the iterative scheme used for the quantitative thermoacoustic imaging

4.2 Example 2

In the previous example, the *a priori* value of ε′ was correct; that is to say, the value of ε′=55 used as the known fixed input parameter in the forward model when run iteratively within the inversion scheme was the same value of ε′ used to generate the simulated measured absorbed power density map. In this example, we demonstrate the effect of ε′ used in the inversion being different to that used to generate the measured absorbed power density map. The measured absorbed power density map was generated for a series of alternating strips of ε′=50 and ε′=58, while the corresponding σ values were 2.14 S/m and 2.57 S/m respectively. A control case was done where both strips had the same value of ε′ = 55 and the σ unchanged at 2.14 S/m and 2.57 S/m respectively. For both cases, noise was present in the form of the reduced number of mesh elements used to generate the simulated measured absorbed power density maps. Also for both cases, the incident electric field has the same orientation as in the previous example. The results are presented in Fig. 4. In Fig. 4A, the true σ distribution is shown while Fig. 4B shows the P_d when the ε′ of both strips is 55. As in the previous example, the absorbed power density map (P_d) shown is before downsampling onto the coarse voxels used in the iteration The P_d when the strips have ε′=50 and ε′=58 is not shown but has a similar profile although with different amplitudes. The result of the reconstruction of σ after 13 iterations is shown in Fig. 4C for the case when the ε′ of both strips is 55. In this case the *a priori* value of ε′ = 55 used in the inversion is correct. When the absorbers now have ε′ values of 50 and 58, the result of the reconstruction of σ is shown in Fig. 4D after 13 iterations. In this case, the *a priori* value of ε′ = 55 used in the inversion is wrong, since the actual ε′ of the absorbers is different. Two vertical slices through Fig. 4C and Fig. 4D is shown in Fig. 4E. The maximum deviation of the recovered conductivity from the true value occurs in the regions where |E| is low for the two cases. The case where the *a priori* ε′ value is incorrect shows greater deviation from the true values, the worst case excursion being about 10% from the true value. The latter suggests that the inversion may not be excessively sensitive to errors in the *a priori* ε' value.

4.3 Example 3

The absorber distributions in the two previous examples were symmetric about the x axis (in order to reduce the computation time) and occupied a significant proportion of the domain under reconstruction. In addition, the only noise present was that due to the reduced number of mesh elements in generating the simulated measured P_d map. In the current example, the absorber distribution was non symmetric and Gaussian noise was added to the absorbed power density map in addition to the non-Gaussian noise due reduction of mesh element when generating P_d. Noise levels of -40dB, -30dB, -20dB relative to the P_d signal power were added. The resulting SNR ranged from 4dB to 54dB, -0.1dB to 45.2dB and -3.0dB to 43.9dB respectively for the three cases. The incident field orientation is the same as previous examples. The results are presented in Fig. 5, with the absorbed power density map (P_d) is shown before downsampling. As expected, as the noise added increases, the recovered σ distribution deviates from the true values. The effect is severe in the areas having low |E|.

5. CONCLUSION

The quantitative reconstruction of the conductivity distribution of absorbers of varying geometries and sizes has been demonstrated. The reconstruction is based on a simple iterative method and requires *a priori* knowledge of the real part of the complex permittivity of the absorber. With certain high water content tissue the assumption of constant real permittivity as used here is reasonable. When imaging a mixture of adipose dominated and high water content tissues, such an assumption of constant real permittivity is not viable due to the significant variation of real permittivity in such tissue. For such situation, by illuminating at two different positions, or frequencies, extra information on the real permittivity distribution can be obtained. A similar approach has been implemented in quantitative photoacoustic image reconstruction[5, 6].

The quantitative reconstruction method described in this paper has been demonstrated using realistic tissue dielectric properties in the presence of both Gaussian and non-Gaussian noise being added to the simulated measured absorbed power density map. The inversion is shown to be stable, even if the guess for the real part of permittivity is incorrect but within a range of physiological values which the real part of permittivity found in soft tissue can take.

REFERENCES

[1] Xu, M., Wang, L.V., Pulsed-microwave-induced thermoacoustic tomography: “Filtered backprojection in a circular measurement configuration”, Med. Phys. 29(8), 1661-1669 (2002)
[2] Polk, C., and Postow, E., [Handbook of biological effects of electromagnetic fields], CRC Press, 1996
[3] Italian National Research Council, Institute for Applied Physics, Available http://niremf.ifac.cnr.it/tissprop/ [Accessed: 3rd October 2011].
[4] Cox, B. T., Arridge, S. R., Kostli, K. P., and Beard, P. C., “Two-dimensional quantitative photoacoustic image reconstruction of absorption distribution in scattering media by use of a simple iterative method," Applied Optics 45(8), 1866-1875 (2006)
[5] Cox, B. T., Arridge, S. R., and Beard, P. C., “Estimating chromophore distribution from multiwavelength photoacoustic images," J. Opt. Soc. Am. 26(2), 443-455 (2009)
[6] Bal, G., Uhlmann, G., “Inverse diffusion theory of photoacoustics,” Inverse Problems 26(8), 085010 (2010)
[7] Yao, L., Guo, G., Jiang, H., “Quantitative microwave-induced thermoacoustic tomography,” Med. Phys. 37(7), 3752-3759 (2010)
[8] Bal, G., Ren, K., Uhlmann, G., Zhou, T., “Quantitative thermo-acoustics and related problems,” Inverse Problems 27(5), 055007 (2011)

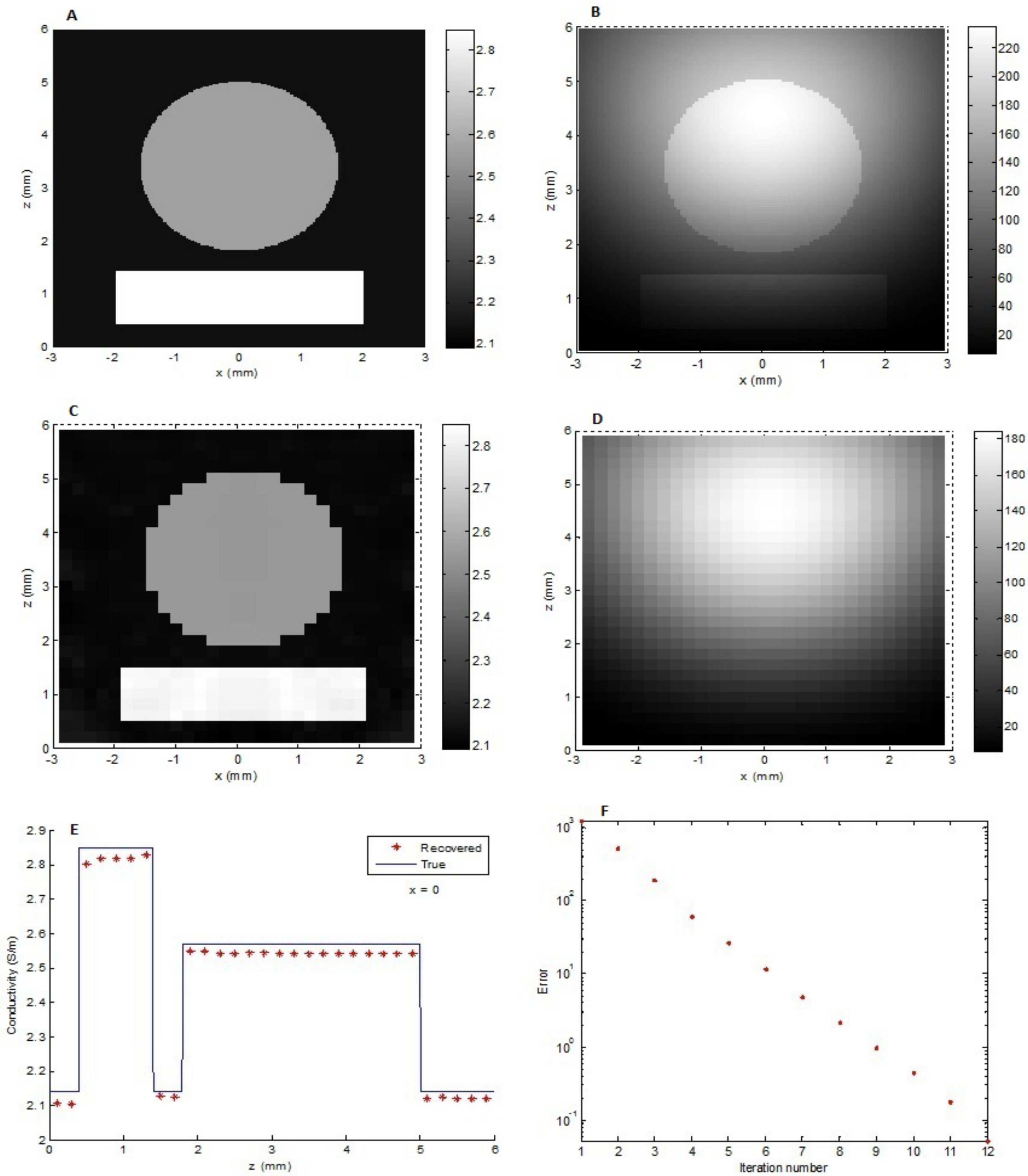

Figure 3. Quantitative reconstruction of absorbers - example 1. (A), true conductivity distribution. σ = 2.57 S/m (circle), 2.85 S/m (rectangle), and 2.14 S/m (background). ε′ = 55. (B) 'measured' P_d (mW/cm^3) before downsampling. (C) recovered conductivity distribution (S/m) after 13 iterations. (D) $|E|^2$ recovered after 13 iterations (E in V/m). (E), vertical slice through true (solid line) and recovered (dotted line) conductivity. (F) error values against iteration showing convergence. Error defined as the difference in conductivity between successive iterations, summed for all pixels.

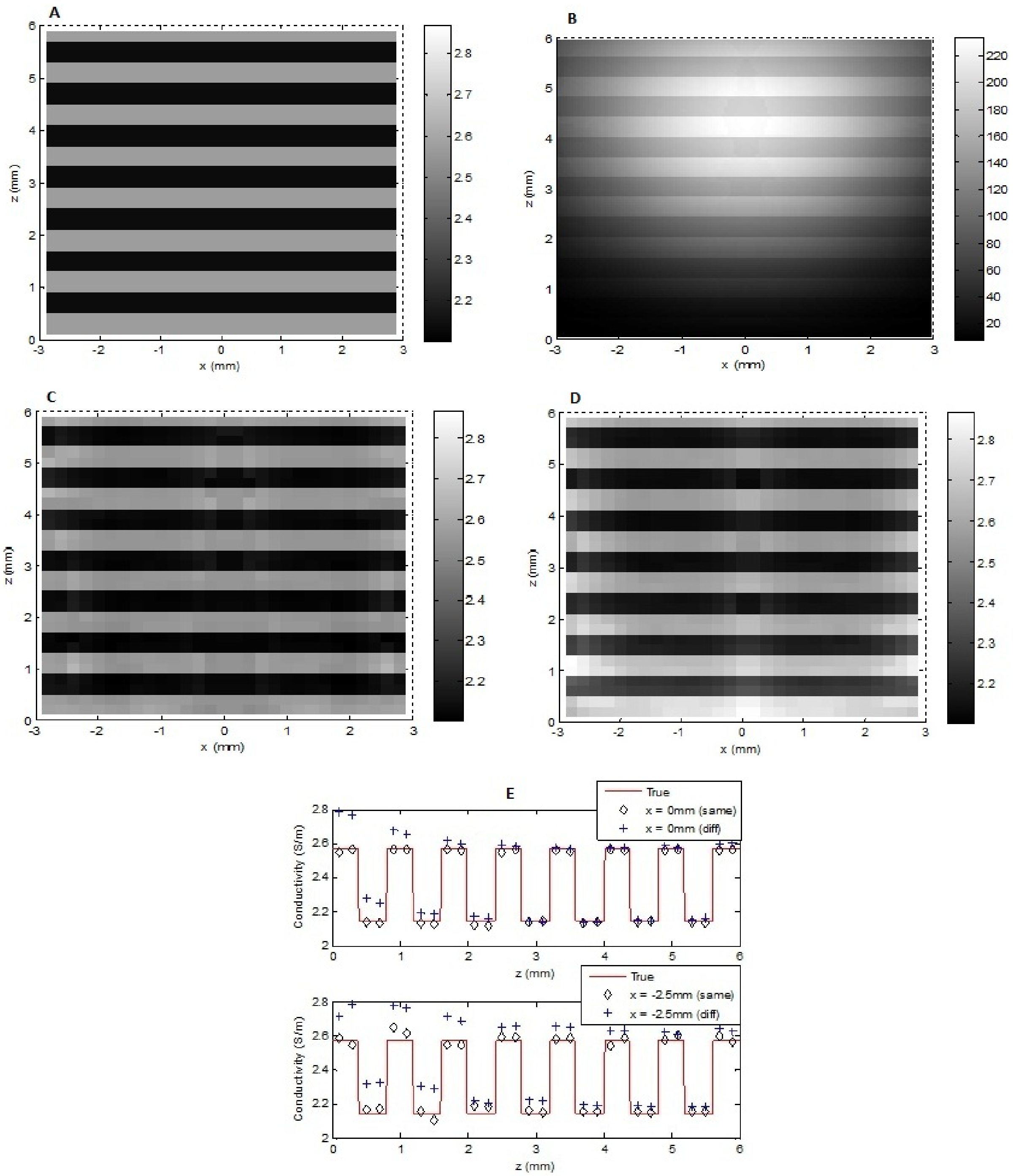

Figure 4. Quantitative reconstruction of absorbers – example 2. (A) true conductivity distribution: 2.57 S/m (yellow strip) and 2.14 S/m (blue strip). (B) 'measured' P_d (mW/cm^3) before downsampling when both strips have ε′ = 55. (C) recovered conductivity distribution (S/m) after 13 iterations when both strips have ε′ = 55. (D) recovered conductivity distribution after 13 iterations when strips have ε′ = 50 and 58 (E) vertical slice through true conductivity (solid), recovered conductivity when both strips have same ε′ (diamond) and recovered conductivity when both strips have different ε′ (cross).

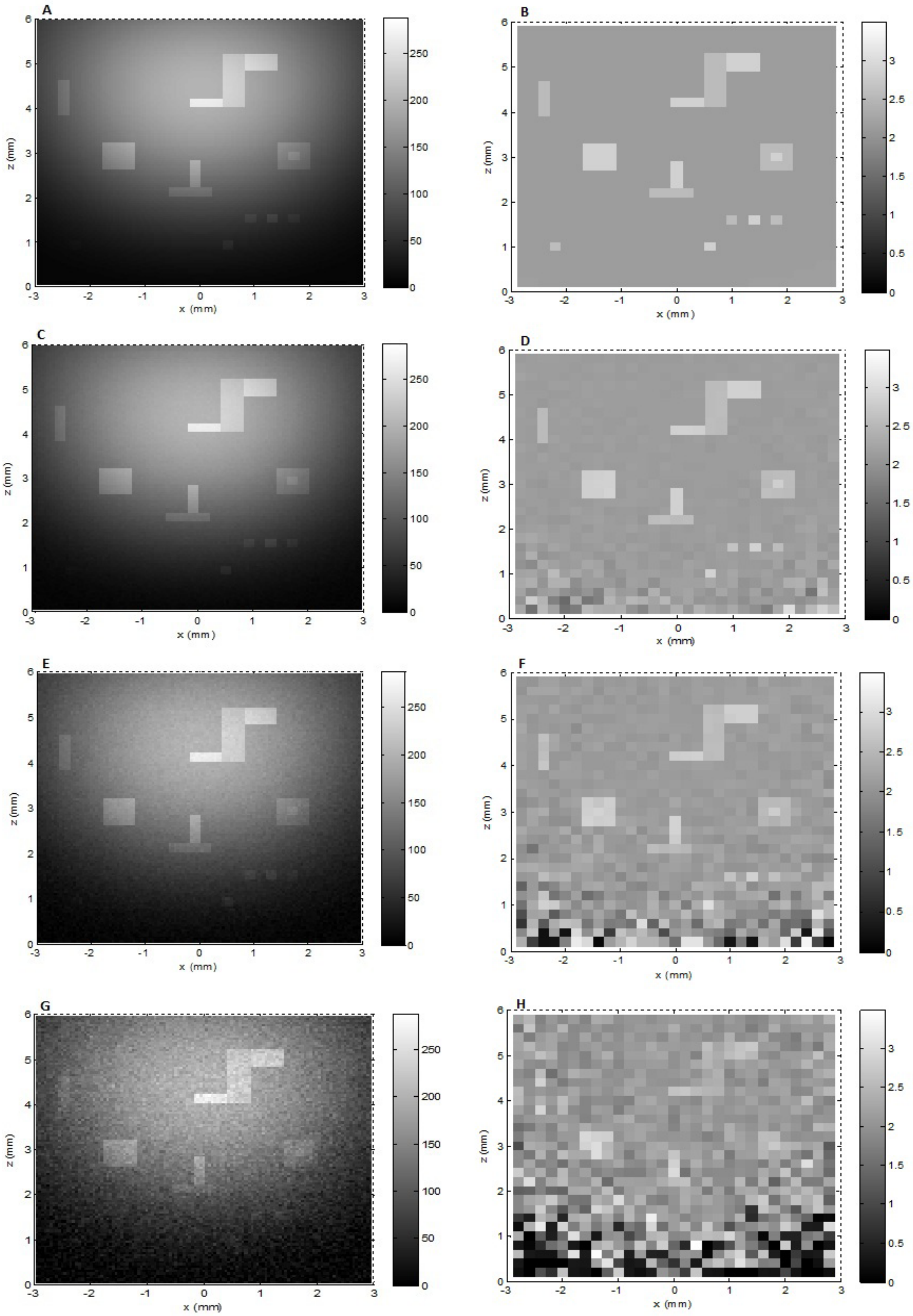
A
B
C
D
E
F
G
H
z (mm)
x (mm)

Figure 5. Quantitative reconstruction of absorbers – example 3. (A) 'measured' P_d (mW/cm^3) containing only down sampling noise before downsampling. (B) conductivity distribution (S/m) recovered from A after 10 iterations. (C) 'measured' P_d before downsampling plus -40dB Gaussian noise power (SNR ranges from 4dB to 54.1dB). (D) conductivity distribution (S/m) recovered from C after 10 iterations. (E) 'measured' P_d before downsampling plus -30dB Gaussian noise power (SNR ranges from -0.1dB to 45.2dB). (F) conductivity distribution (S/m), recovered from E after 10 iterations. (G) 'measured' P_d before downsampling plus -20dB Gaussian noise power (SNR ranges from -3.0dB to 43.9dB). (H) conductivity distribution (S/m), recovered